Egyptian Journal of Radiology and Nuclear Medicine

RESEARCH Open Access

Diffusion-weighted-MRI versus PET-CT in assessment of chest wall lesions

Youssriah Yahia Sabri[1], Ikram Hamed Mahmoud[2], Aya Hussein Muhammed Mabrouk[1], Mostafa Ahmed Kahiry[1], Mohamed Raafat Abd El-Mageed[1], Yasmine Hamdy El Hinnawy[1], Hossam Zawam[1], Amira Aly Hegazy[1] and Sally Fouad Tadros[1*]

Abstract

Background Chest wall lesions comprise benign and malignant etiologies. Numerous classification systems have been proposed based on etiology, origin site, tissue composition and whether the lesion is benign or malignant. Despite that conventional radiological studies are able to provide detailed information about the tumor morphology such as size, location, and extent tissue characteristics, yet, they cannot reliably differentiate benign from malignant neoplasms. This study aimed to detect the diagnostic value of diffusion weighted MRI and PET/CT in evaluating chest wall lesions, and in differentiating benign from malignant lesions.

Results The chest wall lesions were divided into either benign or malignant; 34 cases (47.9%) were diagnosed as benign, while 37 cases (52.1%) were diagnosed as malignant. The mean ADC value of malignant lesions ($0.8 \pm 0.3 \times 10{-}3$ mm2/s) was significantly lower than that of benign lesions ($1.3 \pm 0.6 \times 10{-}3$ mm2/s). This yielded statistically significant results with cut off value of $1.25 \times 10{-}3$ mm2/s for confident diagnosis and differentiation of benign from malignant lesions, with sensitivity of 91.9%, specificity of 70.6%, positive predictive value of 77.27%, negative predictive value of 88.89% and accuracy of 81.7%. The mean SUV of malignant lesions (14.2 ± 6.1) was significantly higher than that of benign lesions (1.5 ± 1.3). This yielded statistically significant results with cut off value of 2.45 for confident diagnosis and differentiation of benign from malignant lesions, with sensitivity of 100%, specificity of 82.4%, positive predictive value of 86.05%, negative predictive value of 100%, and accuracy of 91.5%.

Conclusions Both DWI-MRI and PET/CT can reliably differentiate benign from malignant lesions, yet, PET/CT showed higher sensitivity, specificity and accuracy.

Keywords DWI-MRI, Chest wall, PET-CT

Background

The chest wall represents the structures encircling the lungs. These structures include various tissues, Including cartilage, bone, muscle, fascia, vasculature, lymphatic vessels, fat, and skin [1].

Chest wall lesions comprise benign and malignant etiologies. Numerous classification systems have been proposed based on etiology, origin site, tissue composition and whether the lesion is benign or malignant [1–3].

The following schemes show an overview of the benign (Fig. 1) and malignant (Fig. 2) lesions of the chest wall [2–6].

About 50% to 80% of chest wall tumors are malignant and more than half of them are metastatic in origin [7].

Tumors that originate from the chest wall are uncommon, and unfamiliarity with them cause diagnostic challenges for radiologists. Additionally, the imaging findings

*Correspondence:
Sally Fouad Tadros
sallyfouad86@gmail.com
[1] Kasr Al-Ainy Faculty of Medicine, Cairo University, Al-Manial, Cairo 11559, Egypt
[2] National Cancer Institute, Kasr Al-Ainy Street, Fom El-Kalig, Cairo 11796, Egypt

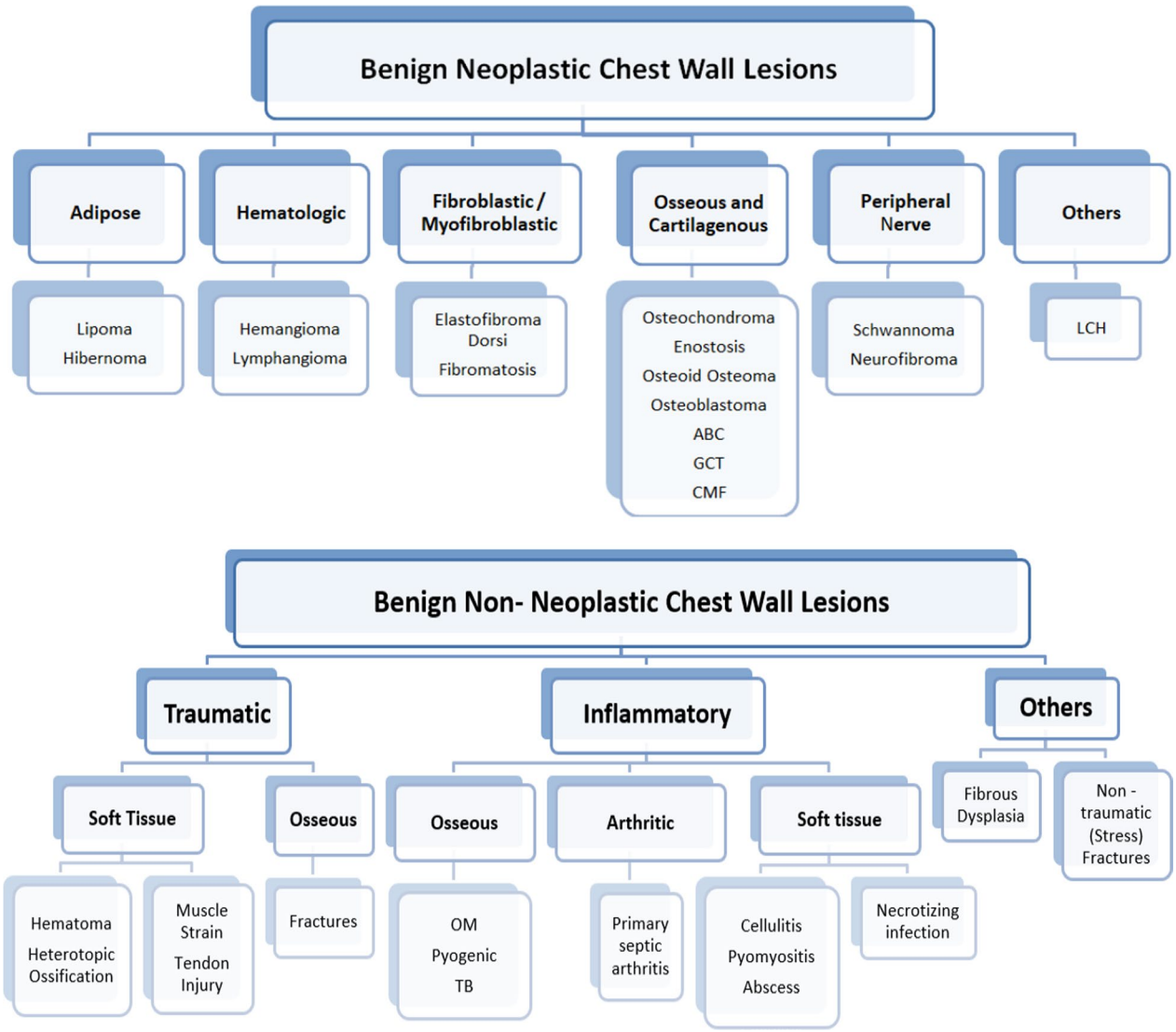

Fig. 1 A scheme showing overview of the benign chest wall lesions. **ABC = Aneurysmal bone cyst, GCT = Giant cell tumor, CMF = Chondromyxoid fibroma, LCH = Langerhan cell histocystosis, OM = Osteomyelitis, TB = Tuberculosis

of most of these neoplasms are non-specific, especially those that are locally aggressive [3].

Despite that conventional radiological studies are able to provide detailed information about the tumor morphology such as size, location, and extent tissue characteristics, yet, they cannot reliably differentiate benign from malignant neoplasms [6].

Diffusion Weighted Imaging (DWI) is a functional Magnetic Resonance Imaging (MRI) technique that has the advantage of being broadly available and non-invasive with short time of acquisition. It has the capability of studying tissue characteristics on the basis of diffusivity of water molecules within them. By calculating the apparent diffusion coefficient (ADC) value, quantitative assessment of a neoplasm is also possible, which is inversely correlated to tissue cellularity [8].

Similarly, 18F Fluorodeoxyglucose Positron Emission Tomography/Computed Tomography (FDG PET/CT) is a non-invasive technique that provides tomographic images as well as quantitative assessment of the metabolic activity of target tissues. FDG accumulates in tissue proportional to the amount of glucose consumption, while, CT allows the visualization of morphological and anatomical structures with high spatial resolution [9, 10].

The study aimed to detect the diagnostic value of diffusion weighted MRI and PET/CT in evaluating chest wall lesions, and in differentiating benign from malignant lesions.

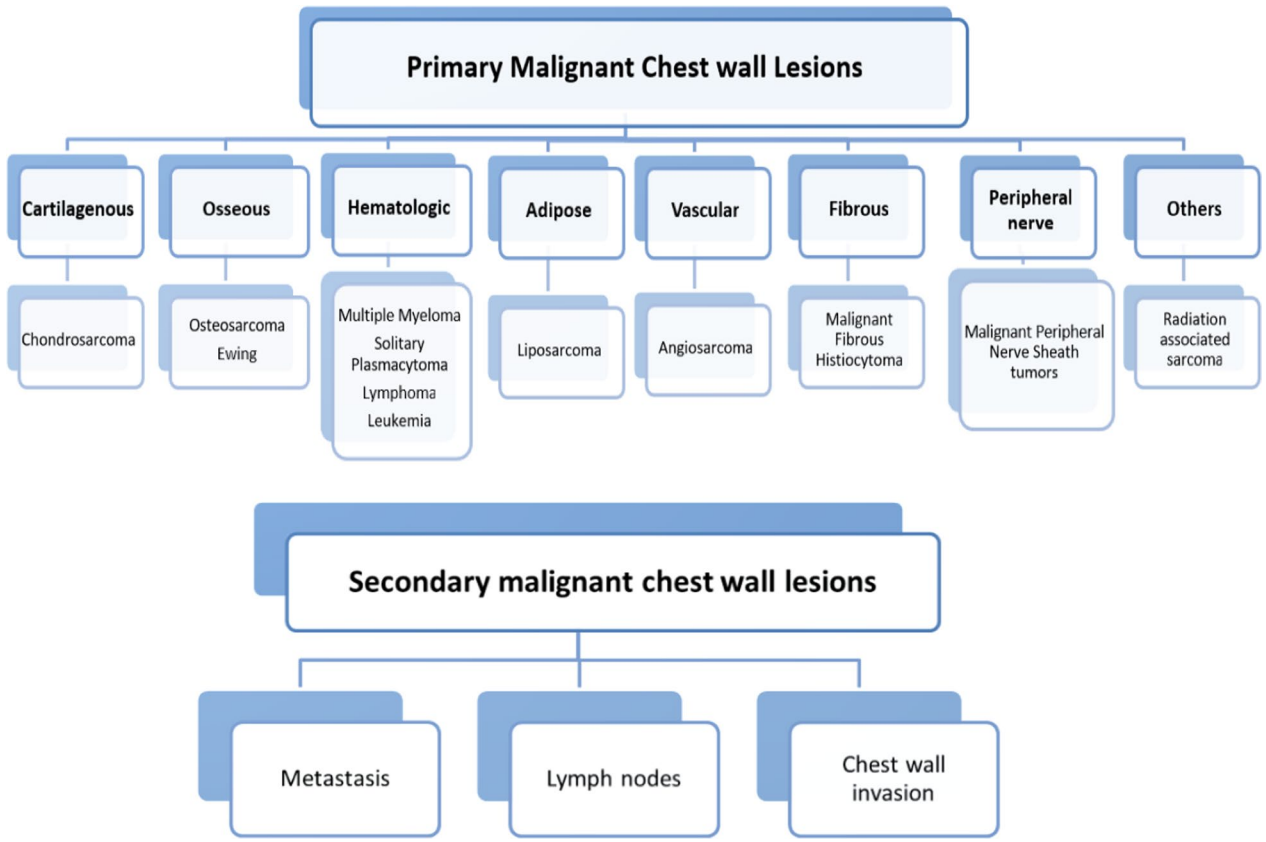

Fig. 2 A scheme showing overview of the malignant chest wall lesions

Methods

This prospective cross-sectional study was approved by our local institutional review board. Informed written consent was obtained from all included participants or their authorized representatives.

Study population

This study included 71 patients; 30 males (42.3%) and 41 females (57.7%), their ages ranged from 2 to 71 (with a mean age of 44 ± 19 years).

The study was conducted over a period of 20 months (from January 2021 to September 2022). Patients were referred from the pulmonology and oncology departments and outpatient clinics to the radiology department to perform MRI of the chest with DWI, and PET/CT for assessment of chest wall lesions.

The most common symptoms reported at presentation were dyspnea, chest pain, deformity and weight loss (Table 1).

All patients performed MRI of the chest with DWI and PET/CT.

Table 1 The presenting symptoms numbers and percentages in our study

Symptoms	Number of patients	Percentage (%)
Dyspnea	44	61.9
Chest pain	40	56.3
Deformity	36	50.7
Weight loss	33	46.4
Cough	21	29.5
Hemoptysis	15	21.1

Inclusion criteria Patients with identified chest wall lesion on clinical examination or CT.

Exclusion criteria

(a) Exclusion criteria for MRI

General exclusion criteria for MRI; for example: claustrophobic patients, patients having a contraindication to MRI (cochlear implants, cerebral aneurysm clips, pacemaker, ocular metallic foreign body, etc.).

(b) Exclusion criteria for PET/CT

General exclusion criteria for PET/CT; for example: pregnant patients, history of insulin-depended diabetes mellitus from clinical notes, etc.

Methods

1. MRI technique

DWI-MRI of the chest was done at our Radiology department with a 1.5T unit (Achieva; Philips Medical Systems, Best, The Netherlands).

(a) Patient preparation

Reassurance, simple clarification of the procedures and instructing the patients not to move during the examination with calm breathing.

Contrast-enhanced MRI was recommended in 51 patients (72.9%). A venous catheter was placed in a peripheral vein (ante-cubital vein in most cases) attached to automatic injector through a long connecting tube to allow easy injection without changing the patient position. The injected dose was 0.1 mmol gadolinium–DTPA/kg. Patients were instructed to fast for six hours, and to perform a renal function test prior to the scan.

(b) Patient position

The patients were placed in a supine position with their heads directed to the scanner bore.

(c) Image acquisition

MRI of the chest was done using a 16-channel phased array torso coil (Sense XL Torso; Philips Healthcare) with respiratory gating. The following sequences were used: axial T1, T2 and STIR WIs, coronal T1 and T2 WIs, sagittal T2 WIs and DWI. DWI was performed in the axial plane, using three b values; low (0–50 s/mm2), intermediate (500 s/mm2) and high b value (1000 s/mm2).

- *Axial T1 WI (TSE)* repetition time/echo time: 10 ms/4.6 ms; direction of frequency encoding: AP; section thickness: 9 mm; gap: 2 mm; field of view: 420 × 325 × 306 mm; matrix: 212 × 179.
- *Coronal T1 WI (TSE)* repetition time/echo time: 10ms/4.6ms; direction of frequency encoding: R/L; section thickness: 9 mm; gap: 1.5 mm; field of view: 425 × 425 × 208 mm; matrix: 284 × 246.
- *Axial T2 WI (TSE)* repetition time/echo time: 738 ms/100 ms; direction of frequency encoding: AP; section thickness: 9 mm; gap: 2 mm; field of view: 420 × 325 × 306 mm; matrix: 248 × 167.
- *Coronal T2 WI (TSE)* repetition time/echo time: 738 ms/100 ms; direction of frequency encoding: R/L; section thickness: 9 mm; gap: 1.5 mm; field of view: 425 × 425 × 208 mm; matrix: 284 × 246.
- *Sagittal T2 WI (TSE)* repetition time/echo time: 738 ms/100 ms; direction of frequency encoding: AP; section thickness: 8.5 mm; gap: 1 mm; field of view: 400 × 299 × 284 mm; matrix: 268 × 195.
- *STIR WI* repetition time/echo time: 1788.3ms/20ms; direction of frequency encoding: AP; section thickness: 10 mm; gap: 2 mm; field of view: 450 × 333 × 334 mm; matrix: 216 × 161.
- *DWI (SS-SE-EPI-with fat suppression)* acquired in a transverse plane, using three b values; low (0–50 mm^2/s), intermediate (500 mm^2/s) and high b value (1000 mm^2/s); repetition time/echo time: 1407 ms/66.5 ms; direction of frequency encoding: AP; slice thickness: 9 mm; inter-slice gap: 2 mm; field of view: 420 × 324 × 306 mm; matrix: 140 × 107.
- *The apparent diffusion coefficient (ADC) maps* were calculated by the MR system via linear regression analysis of the natural log of signal intensity using all three b-values (0, 500 and 1000 mm^2/s).

(d) Image analysis

Both qualitative and quantitative analysis of the depicted chest wall lesions was done by visually assessing the different pulse sequences and by measuring their ADC values respectively.

(i) Qualitative assessment

Chest wall diseases were analyzed for the number of lesions, site, size, shape, morphological features, tissue characterization, extent and their relation to adjacent structures.

We considered lymph nodes enlarged if they were > 10 mm in short-axis diameter.

We reviewed each lesion signal intensity in the different pulse sequences with comparison of their signal relative to the muscles signal in the same pulse sequence. We also qualitatively assessed the lesions on DWI and ADC maps by inspecting their signal intensity on the high-b-value (b = 1000 mm^2/s) DWI and correlating it to that on the corresponding ADC map. Associated MR imaging findings were also recorded.

(ii) Quantitative assessment

Measuring ADC values was done by placing the region of interest (ROI) within the center of the lesion on the ADC maps with an effort to avoid interference from the surrounding lung tissue and vascular structure.

In case of soft tissue lesions, the ROI was placed within the most restricted areas (excluding apparent cystic/necrotic areas).

To avoid the possible magnetic susceptibility artifacts, ADC values were computed far from lung-fluid interfaces and diaphragmatic areas.

2. Positron emission tomography/computed tomography technique

(a) Patient preparation
We asked the patients to fast for six hours before the scan, and to do a renal function test. We also asked the patients to remove any metallic items, and they were given a gown to wear. We inserted an I.V. cannula in the patient's arm for ^{18}F FDG administration. We instructed the patients to avoid any strenuous activity after the ^{18}F FDG injection to avoid physiologic FDG muscle uptake, and to void before scanning.
For known diabetic patients, we measured the serum glucose before injection of ^{18}F FDG, and fasting levels were 70–180 ng/dl. Diabetic patients were instructed not to have their regular insulin administered within four hours of FDG administration.
In order to decrease brown fat, a warm environment was provided to the patients before injection of ^{18}F FDG and the patients were instructed to follow a high-fat, low-carbohydrate, protein-permitted diet prior to the examination.

(b) Dosage administration
Before the examination by 45–90 min, we injected 10-20mCi (370 MBq; approximate dose to patient, 3-5MBq/Kg) ^{18}F FDG. This duration is the uptake phase in which the FDG is bio-distributed and transported into the patient's cells. We asked the patients to rest in a quiet room, and to minimize their movements, including talking in order to decrease the FDG physiologic uptake into skeletal muscle, which can be confusion during scan the interpretation.

(c) Patient position
We positioned the patients in a comfortable head fixation with their arms up.

(d) Image acquisition
A low dose non enhanced CT scan was performed first, followed by a whole-body PET study, then a whole-body contrast-enhanced CT using Siemens Biography 265 Multi-slice PET/CT scanner. The duration of the study was approximately 20–30 min. The scanning started from the skull base and extended caudally to the level of the upper thighs (brain, neck, chest, abdomen and pelvis). Scanning parameters were a collimator width of 5.0 mm, pitch of 1.5, gantry rotation time of 0.8 s, and field of view of 50 cm. Reconstruction of the helical data was done at 1 mm intervals.

(i) CT technique
The contrast-enhanced CT was performed following injection of 1–2 ml/Kg of a low-osmolarity iodinated contrast medium at a rate of 4 ml/sec by using a power injector.

(ii) PET technique
PET was performed following the CT study without moving the patient. About six to seven bed positions are programed in the three-dimensional acquisition mode to scan the whole patient with 3–5-min acquisition at each bed position.

(iii) PET/CT fusion
Axial PET and CT images were taken then reconstructed into coronal and sagittal images to enhance image analysis. Corresponding "fusion" images were then generated by combining the data of the PET and CT images.
The duration of an integrated PET/CT scan was about 25 min.

(e) Image analysis
The CT scans were interpreted by experienced radiologists and the PET/CT scans were separately interpreted by a consensus of two experienced nuclear medicine radiologists. A ROI of 5 to 10 mm was placed manually over the area of maximal activity on slices within the tumor and the standardized uptake value (SUV) was calculated.
Pathological ^{18}F FDG uptake was described as accumulation of radiotracer outside the normal anatomic structures of higher intensity than background activity.
The CT and fused PET/CT images were assessed for the presence chest wall lesions, their number, site, size, shape, and relation to the surroundings. Chest wall infiltration was defined as soft tissue infiltration by the tumor and/or lytic destruction of the ribs or vertebrae.
Lymph nodes showing increased FDG uptake were characterized as positive for metastasis even if they were smaller than 1 cm in their short-axis diameter. However, lymph nodes with little or no FDG uptake were considered benign, even if they were larger than 1 cm in their short-axis diameter.

Histopathological diagnosis

The final diagnoses were established by histopathological examination whenever needed [46 patients (64.8%); 34 were CT guided (73.9%), and 12 were US guided (26.1%)].

The mode of acquisition of the biopsy was determined according to accessibility of the lesions. The rest of cases (35.2%) were diagnosed based on clinical data and typical radiological features.

Statistical analysis

Data was entered on the computer using Microsoft Office Excel Software Program 2019. Data was then transferred and entered into the Statistical Package of Social Science Software program, version 26 (SPSS) to be statistically analyzed. Quantitative variables were summarized as mean, standard deviation, median, and IQR, compared using Mann Whitney U test, where p value < 0.05 was considered significant. Qualitative variables were summarized as frequency and percentage. ROC curve was constructed with area under curve analysis performed to detect best cutoff value of ADC and SUV for detection of malignancy. *P*-values less than 0.05 were considered as statistically significant.

Results

This study included 71 patients; 30 males (42.3%) and 41 females (57.7%), their ages ranged from 2 to 71 (with a mean age of 44 ± 19 years).

The chest wall lesions were divided into either benign or malignant; 34 cases (47.9%) were diagnosed as benign, while 37 cases (52.1%) were diagnosed as malignant.

(A) Benign lesions

The benign lesions were further categorized into benign neoplastic chest wall lesions (27 patients, 79.5%), and benign non-neoplastic lesions (7 patients, 20.5%).

The benign neoplastic lesions were further categorized according to tissue of origin as shown in (Table 2).

The benign non-neoplastic lesions were further categorized according to etiology (Table 3).

Table 3 Classification of benign non-neoplastic lesions according to etiology

Etiology	Lesion	Number of cases	%	Mean ADC value	Mean ADC value
Inflammatory	Abscess	6	8.5	0.75	2.9
Others	Post-operative seroma	1	1.4	2.4	0

(B) Malignant lesions

The malignant lesions were further categorized into primary malignant chest wall lesions (21 patients, 73%), and secondary malignant chest wall lesions (16 patients, 27%).

The primary malignant lesions were further categorized according to tissue of origin as shown in (Table 4).

Secondary malignant lesions were further categorized according to their site (Table 5).

The mean ADC value of malignant lesions ($0.8 \pm 0.3 \times 10^{-3}$ mm^2/s) was significantly lower than that of benign lesions ($1.3 \pm 0.6 \times 10^{-3}$ mm^2/s). This yielded statistically significant results with cut off value of 1.25×10^{-3} mm^2/s for confident diagnosis and differentiation of benign from malignant lesions, with sensitivity of 91.9%, specificity of 70.6%, positive predictive value of 77.27%, negative predictive value of 88.89% and accuracy of 81.7%

The mean SUV of malignant lesions (14.2 ± 6.1) was significantly higher than that of benign lesions (1.5 ± 1.3). This yielded statistically significant results with cut off value of 2.45 for confident diagnosis and differentiation of benign from malignant lesions, with sensitivity of 100%, specificity of 82.4%, positive predictive value of 86.05%, negative predictive value of 100%, and accuracy of 91.5%.

Table 2 Classification of benign neoplastic lesions according to tissue of origin

Tissue origin	Lesion	Number of cases	%	Mean ADC value	Mean SUV value
Adipose	Lipoma	4	4.6	0.43	0.68
Hematologic	Vascular malformation	1	1.4	2.2	1.03
	Lymphatic malformation	2	2.8	2.6	1.01
Fibroblastic/ Myofibroblastic	Fibromatosis	1	1.4	1.5	2.2
	Elasto-fibroma dorsi	18	25.4	1.39	1.04
	Fibrous dysplasia	1	1.4	1.45	6.5

Table 4 Classification of primary malignant lesions according to tissue of origin

Tissue origin	Lesion	Number of cases	%	Mean ADC value	Mean SUV value
Osseous	Osteosarcoma	4	4.6	0.75	12.8
	Ewing/PNET	8	11.3	0.65	15.7
Hematologic	Lymphoma	3	4.2	0.97	9.4
	Multiple myeloma	2	2.8	1.05	4.1
Fibroblastic/ myofibroblastic	UPS	3	4.2	0.93	25.7
Peripheral Nerve	MPNST	1	1.4	0.3	25.2

PNET = Primitive neuroectodermal tumors, UPS = Undifferentiated pleomorphic sarcoma, MPNST = Malignant peripheral nerve sheath tumor

Table 5 Classification of secondary malignant lesions according to their site

Site	Lesion	Number of cases	%	Mean ADC value	Mean SUV value
Direct chest wall invasion	Breast	3	4.5	1.2	13.7
	Lung	1	1.4	1.1	20.5
	Pleura (mesothelioma)	2	2.8	0.6	12.8
	Thyroid	1	1.4	0.6	15.4
Distant metastasis from	Breast	5	7	0.8	13.1
	Lung	3	4.2	0.87	12.3
	Ovary	1	1.4	0.4	4.1

Discussion

Chest wall tumors account for less than 5% of all thoracic neoplasms and represent a heterogeneous group of lesions that can be difficult to diagnose [11] with the new developments in MR systems, DW-MRI of the chest became an emerging functional MRI technique that makes the analysis of tissue characteristics possible on the basis of water molecules diffusivity within tissues [8, 12]. In addition, FDG PET/CT has been found to be more sensitive than CT or MRI in assessing treatment response and prognosis by simultaneously depicting primary lesions and distant metastases on a single scan [13]. This cross section study involved 71 patients; 30 males and 41 females, with age range of 2–71 years (mean age of 44 years).

In this study, the mean ADC value of malignant lesions ($0.8 \pm 0.3 \times 10^{-3}$ mm^2/s) was significantly lower than that of benign lesions ($1.3 \pm 0.6 \times 10^{-3}$ mm^2/s) with cut off value of 1.25×10^{-3} mm^2/s for confident diagnosis and differentiation of benign from malignant lesions, with sensitivity of 91.9%, specificity of 70.6%, and accuracy of 81.7%

Our results are similar to Lim et al. [14], who studied the role of DW-MRI in differentiating between benign and malignant tumors in 65 cases, and concluded that the mean ADC values for benign and malignant soft tissue tumors were 1.689 and 0.965×10^{-3} mm^2/s respectively with statistically significant difference between them (P value < 0.001), showing a cut off value of 1.2×10^{-3} mm^2/s that yielded a sensitivity of 92%, specificity of 87%, and accuracy of 90%.

Our results are however, slightly different from Lee et al. [15], who concluded that the mean ADC values for benign and malignant soft tissue tumors were 1.47 and 1.17×10^{-3} mm^2/s respectively, with a cut off value of 1.31×10^{-3} mm^2/s that yielded a sensitivity of 74%, specificity of 73%, and accuracy of 74%.

We encountered in our study 4 patients with benign lesions showing morphological, anatomical and signal characteristics of lipomas, yet, demonstrating very low ADC value (mean value of 0.43×10^{-3} mm^2/s), similar to those of malignant soft-tissue masses (Fig. 3). These results are consistent with those of Hassanien et al. [16], Dietrich et al. [17] and Einarsdóttir et al. [17], who stated that there is some overlap between benign and malignant soft tissue tumors such as in lipomas, giving low ADC values similar to malignant lesions (false positive). According to Hassanien et al. [16], the 5 lipomas included in their study had a mean ADC value of 0.31×10^{-3} mm^2/s [16–18].

There were 18 elastofibroma dorsi cases included in our study showing facilitated diffusion; their mean ADC value was 1.39×10^{-3} mm^2/s (Fig. 4). On surfing the literature, studies performed to diagnose the role of DWI on elastofibroma cases were quite limited. Tsubakimoto et al. [19], performed a study on 41 elastofibroma cases, and concluded that none of the lesions had true diffusion restriction; their mean ADC value was 1.36×10^{-3} mm^2/s, which is similar to our results.

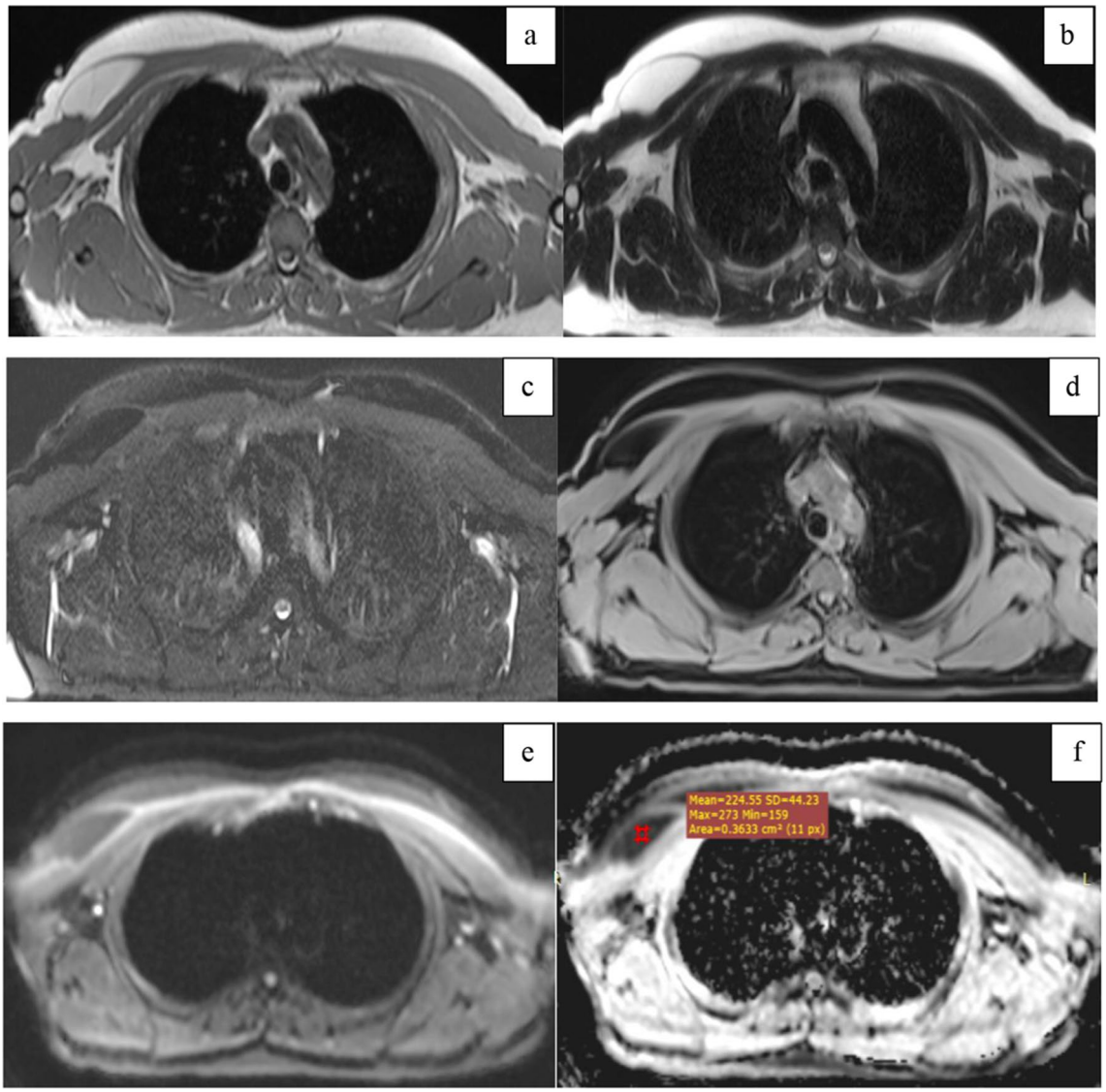

Fig. 3 38-year-old male patient complaining of right anterior chest wall swelling. **a** Axial T1, **b** axial T2, **c** axial T2 fat suppression, and **d** post contrast axial T1 fat suppression showing right pectoralis major intra muscular well-defined lesion eliciting signal intensity identical to fat in T1 and T2 WIs with drop of signal in fat suppressed image and no post contrast enhancement. **e** DWI and **f** ADC map showing low DWI signal intensity with corresponding low signal in ADC map. ADC value = 0.2×10^{-3} mm^2 /s

Our results demonstrated that vascular malformations (1 case) and lymphatic malformations (2 cases) had ADC values higher than other benign tumors with mean ADC value of 2.4×10^{-3} mm^2/s. These results are consistent with those of Hassanein et al. [16], who studied 3 hemangioma cases included in their research, and found that the mean ADC value of these lesions was 2.45×10^{-3} mm^2/s.

Regarding the single fibromatosis case included in our study, the mean ADC value was 1.5×10^{-3} mm^2/s, which is comparable to Zeitoun et al. [20], Oka et al. [21], and Pekcevik et al. [22] studies. Zeitoun et al. [20] performed a study on 40 pathologically proven fibromatoses lesions, and revealed mean ADC value of 1.41×10^{-3} mm^2/s [20–22].

Concerning the inflammatory chest wall lesions included in our study, the mean ADC value of abscesses was 0.75×10^{-3} mm^2/s. This is coherent to Kumar et al. [23] and Douis et al. [24]; the latter mentioned that false positive cases included abscesses, as they may result in restricted diffusion with low ADC values, hence, overlapping with the ADC values for malignant soft tissue lesions [23, 24] (Fig. 5). However, the typical clinical presentation of inflammatory signs such are skin redness and

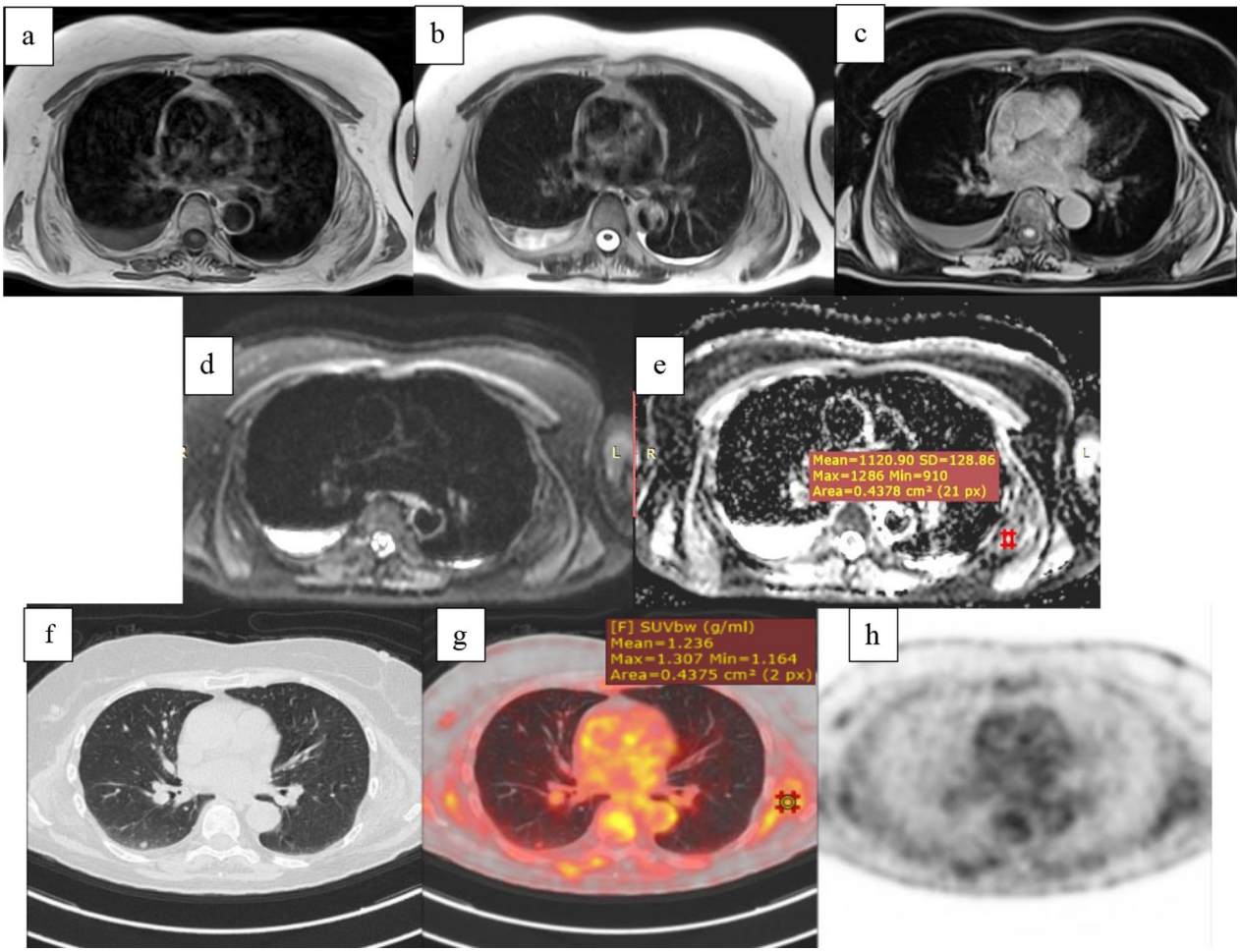

Fig. 4 67-year-old female patient with past history of uterine cancer complaining of bilateral infra-scapular fullness. MRI chest and PET/CT were performed as part of her investigation profile with incidental discovery of bilateral elastofibroma dorsi; larger on the left side. **a** Axial T1, **b** axial T2, and **c** post contrast axial T1 fat suppression showing bilateral sub-scapular soft tissue lesions deep to the serratus anterior and latissimus dorsi muscles exhibiting lamellar feathery pattern, and signal intensity similar to the adjacent muscles on T1 and T2 WIs with patchy enhancement. Mild right and minimal left pleural effusions were also noted. **d** DWI and **e** ADC map showing low DWI signal intensity with corresponding low signal in ADC map. ADC value = 1.1×10^{-3} mm^2/s. **f** Axial CT, **g** axial fused PET-CT, and **h** axial PET image showing FDG activity within bilateral elastofibroma (SUV = 1.2). Note FDG uptake in incidentally discovered right lower lung lobe nodule that was not seen in the chest MRI

hotness in addition of the characteristic imaging features of uniform marginal enhancement with stranding of the surrounding fat planes prevents the misdiagnosis of these lesions.

A single case of post-operative fluid collection (mastectomy surgical bed seroma) was included in our study with mean ADC value 2.4×10^{-3} mm^2/s. Ultrasound guided aspiration of this fluid collection was performed, and yielded benign nature. Our results were compatible with Aktas et al. [25], who performed a study on 42 patients to detect the role of DWI and ADC in differentiating post-operative cancer recurrence from post-operative sequalae as hematoma or seroma, and concluded that the mean ADC value of post-operative benign collections was 2.72×10^{-3} mm^2/s, which was significantly higher than the ADC values of tumor recurrence (1.44×10^{-3} mm^2/s).

Mean ADC values obtained in Ewing sarcoma cases included in our study population yielded an average of 0.65×10^{-3} mm^2/s, which is comparable to that reported by Saleh et al. [26], whose study included 51 pathologically proven Ewing sarcoma cases, with a mean ADC value of $0.71 \pm 0.16 \times 10^{-3}$ mm^2/s.

Note that one of the Ewing sarcoma cases in our study showed mean ADC value of 1.4×10^{-3} mm^2/s, which is considered higher than the average ADC for this lesion

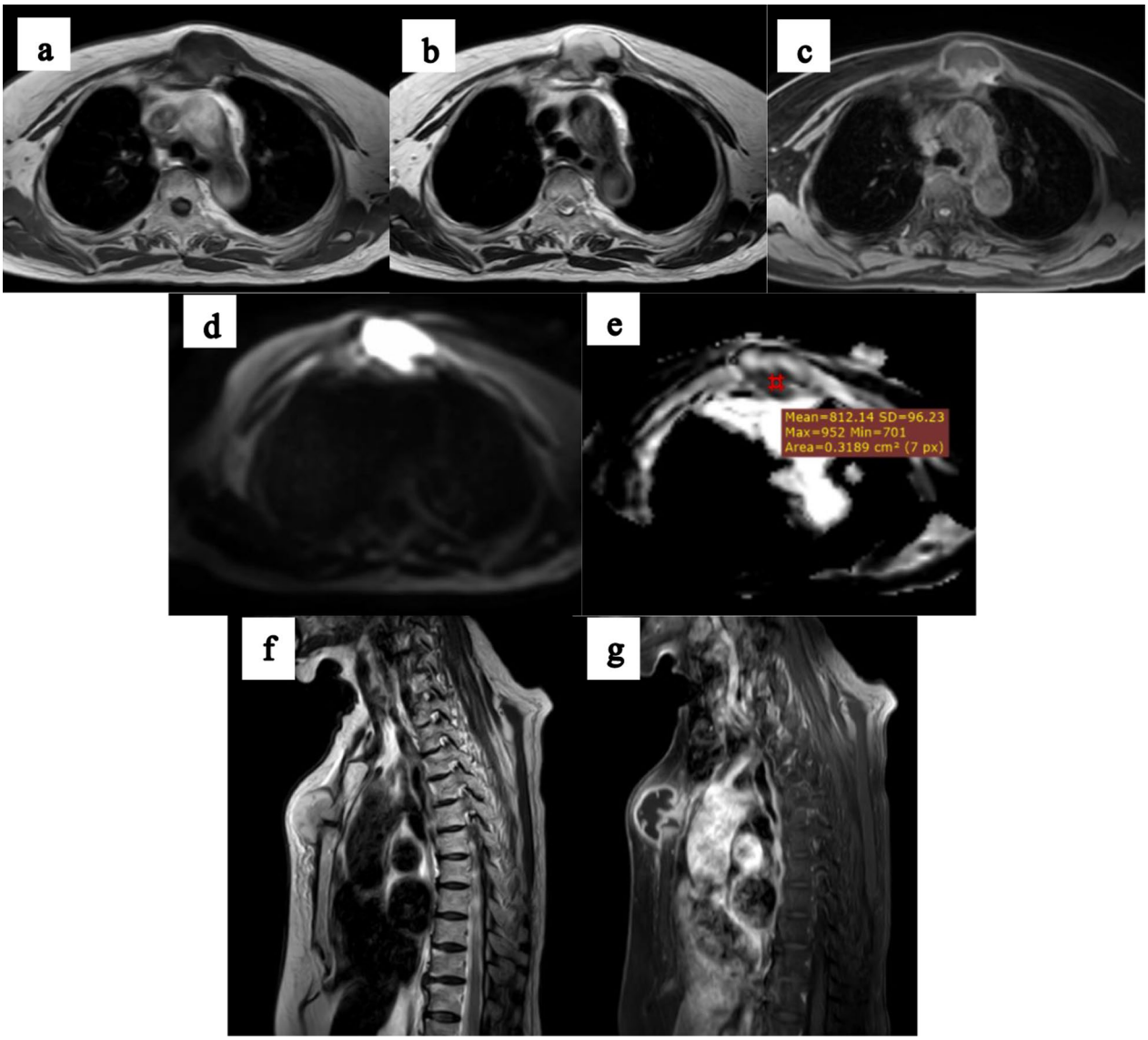

Fig. 5 37-year-old diabetic male patient complaining of anterior chest wall swelling with overlying skin redness. **a** Axial T1, **b** axial T2, and **c** post contrast axial T1 fat suppression showing pre-sternal well-defined subcutaneous lesion eliciting low T1 and high T2 WIs signal intensity with marginal post contrast enhancement. **d** DWI and **e** ADC map showing diffusion restriction in the form of high diffusion signal and low ADC. ADC value = $0.8 \times 10–^{3}$ mm^2/s. **f** Sagittal T2, and **g** Sagittal post contrast T1 fat suppression showing involvement of the underlying bone with no intra-thoracic extension

(Fig. 6). This may be attributed to treatment as the patient received neoadjuvant chemotherapy, therefore internal areas of breakdown were noted within the tumor resulting in high ADC values. Again, these results were comparable to Saleh et al. [26], who compared the ADC values of Ewing sarcoma pre and post therapy, and noted that there is an increase in the ADC value post treatment ($1.6 \pm 0.39 \times 10^{-3}$ mm^2/s).

The mean ADC value of the 4 cases of osteosarcoma included in our study was 0.75×10^{-3} mm^2/s. Likewise, Yakushiji et al. [27] studied 17 cases of osteosarcoma and found that their mean ADC value was $0.84 \pm 0.15 \times 10^{-3}$ mm^2/s.

The mean ADC value of the 3 malignant fibrous histiocytoma cases included in our study was 0.93×10^{-3} mm^2/s. Similarly, Hassanien et al. [16] study included 4 cases of the same lesion with a mean ADC value of $0.81 \pm 0.15 \times 10^{-3}$ mm^2/s.

A single case of MPNST was included in our study with an ADC value range of $0.2–0.4 \times 10^{-3}$ mm^2/s.

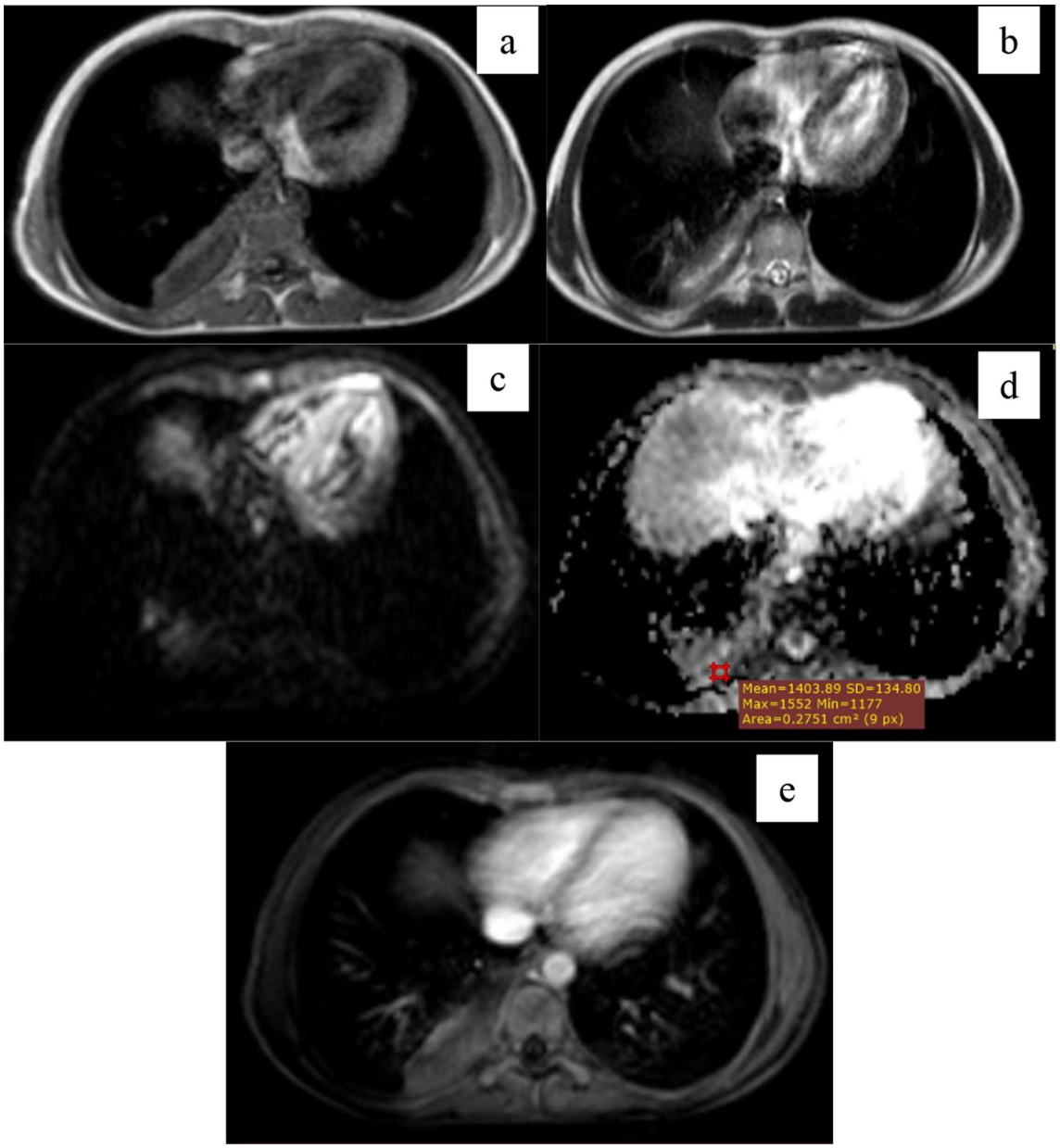

Fig. 6 19-year-old male with pathologically proven right chest wall Ewing sarcoma following neoadjuvant chemotherapy. **a** Axial T1, **b** axial T2, and **e** post axial T1 fat suppression, showing right posterior chest wall pleural-based ill-defined mass lesion eliciting heterogeneous mixed low/intermediate T1 and high/intermediate T2 signal intensities with faint heterogeneous post contrast enhancement. **c** DWI and **d** ADC map showing low DWI signal intensity with corresponding high signal in ADC map. ADC value = 1.4×10^{-3} mm^2/s

Correspondingly, Ahlawat et al. [28] performed a study on 55 cases of peripheral nerve sheath tumor to detect the sensitivity of ADC in differentiating benign from malignant peripheral nerve sheath tumors and concluded that malignant peripheral nerve sheath tumors showed mean ADC value of $0.6 \pm 0.2 \times 10^{-3}$ mm^2/s as compared to benign nerve sheath tumors, which showed mean ADC value of $1.6 \pm 0.4 \times 10^{-3}$ mm^2/s.

The mean ADC value the 2 multiple myeloma cases included in our study was 1.05×10^{-3} mm^2/s. This is higher than the results of Patrenain et al. [29], who performed a study on 27 multiple myeloma cases, and concluded that their mean ADC values was 0.65×10^{-3} mm^2/s.

The mean ADC value of the 3 lymphoma cases included in our study was 0.97×10^{-3} mm^2/s. This is

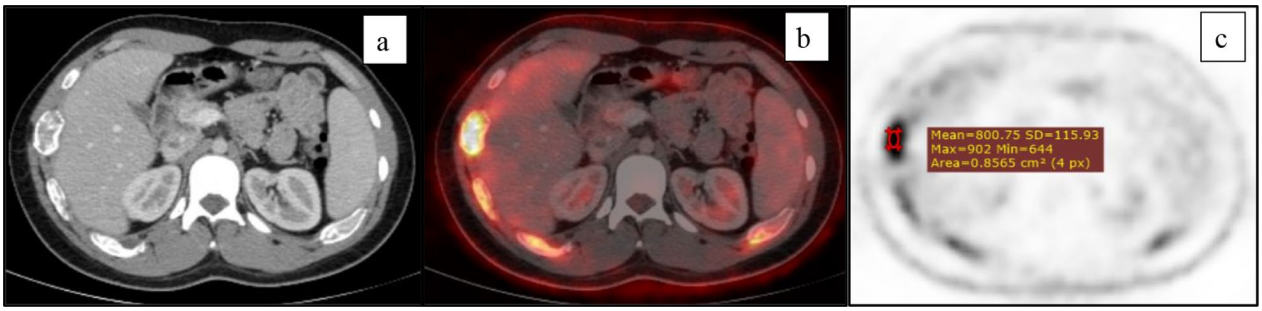

Fig. 7 40-year-old male patient complaining of right chest wall pain and hard swelling. **a** Axial CT, **b** axial fused PET-CT, and **c** axial PET image showing diffuse medullary expansion of several right ribs along the course of the rib with intact cortex and intense FDG uptake corresponding to the affected ribs (SUV = 8). Note the affection of a left rib too. CT-guided biopsy revealed fibrous dysplasia

slightly higher than the results yielded by Surov et al. [30], who performed a study on 14 cases pathologically diagnosed as lymphoma, with mean ADC value of 0.76×10^{-3} mm^2/s.

Most of the secondary malignant lesions encountered in our study were morphologically heterogeneous. This is attributed to several factors, such as the aggressiveness and cellularity of the primary tumor, the areas of hemorrhage and necrosis usually seen in these lesions, and whether the patient started receiving radiotherapy/chemotherapy sessions or not, which has led to a wide range of ADC values. We did our measurements from the solid most homogeneous parts of the tumor, and tried our best not to include cystic or necrotic areas. The minimum ADC value was detected in ovarian metastasis (0.4×10^{-3} mm^2/s), while the highest ADC value was detected in direct invasion from breast cancer (1.2×10^{-3} mm^2/s). The overall mean ADC value of secondary malignant chest wall lesions was 0.82×10^{-3} mm^2/s. Our results are more or less similar to Ahlawat et al. [31], whose study included 8 cases of secondary lesions from different sites, with a minimum ADC value of 0.6, a maximum ADC value of 1.5, and mean ADC value of 1.03×10^{-3} mm^2/s. Note that the average ADC value detected was still lower than that of most benign lesions, thus, allowing differentiation of benign and malignant lesions by ADC.

The mean SUV of the 18 elastofibroma cases included in our study was 1.04 (Fig. 4). This is more or less agrees with Onishi et al., 2011, who performed a study on 34 patients to study the SUV uptake in a total of 75 elastofibroma lesions, with mean SUV of 2.0 ± 0.63 [32].

All inflammatory lesions included in our study showed high FDG uptake. This was due to increased glucose utilization by the inflammatory cells, leading to increased FDG uptake in the affected region. Macrophages play a central role in the host response to injury and infection, and their energy is predominantly supplied by means of intracellular glucose metabolism, hence, causing FDG uptake and consequently false positive results.

The single case of post-operative fluid collection (mastectomy surgical bed seroma) included in our study which was pathologically proven as benign showed no FDG uptake.

Our study included 1 case of fibrous dysplasia, which showed increased FDG uptake (SUV = 6.5, which is above the cut off value) (Fig. 7). These results are conforming to Aoki et al. [33], whose results also showed increased FDG uptake in some of the fibrous dysplasia cases included in their study, exceeding the cut off value, leading to false positive result.

In this study, the mean SUV of malignant lesions (14.2 ± 6.1) was significantly higher than that of benign lesions (1.5 ± 1.3), with cut off value of 2.45, with sensitivity of 100%, specificity of 82.4%, and accuracy of 91.5%.

Our results are close to Feldman et al. [34], who performed a study on 45 patients to detect the role of FDG PET/CT in detection and analysis of musculoskeletal lesions, and concluded a sensitivity of 91.7%, specificity of 100% and accuracy of 91.7% in differentiating benign from malignant lesions. Our results are also more or less compatible with Etchebehere et al. [35] 2016, who performed a meta-analysis including 14 articles composed of 755 patients with 757 soft tissue lesions, to study the role of PET/CT in diagnosis and differentiation of benign and malignant soft tissue lesions. They concluded a sensitivity of 96%, a specificity of 77% and accuracy of 88%.

Our results are however, different from Shin et al. [36], who performed a study to detect the role of PET/CT in differentiating benign from malignant lesions. They concluded a sensitivity of 80%, specificity of 65.2% and accuracy of 73%. Our results are also different from Ioannidis et al. [37], who performed a meta-analysis including 15 studies with 441 soft-tissue lesions (227 malignant, 214 benign), to study the role of FDG PET/CT in diagnosis, differentiation and grading of soft tissue sarcomas, and

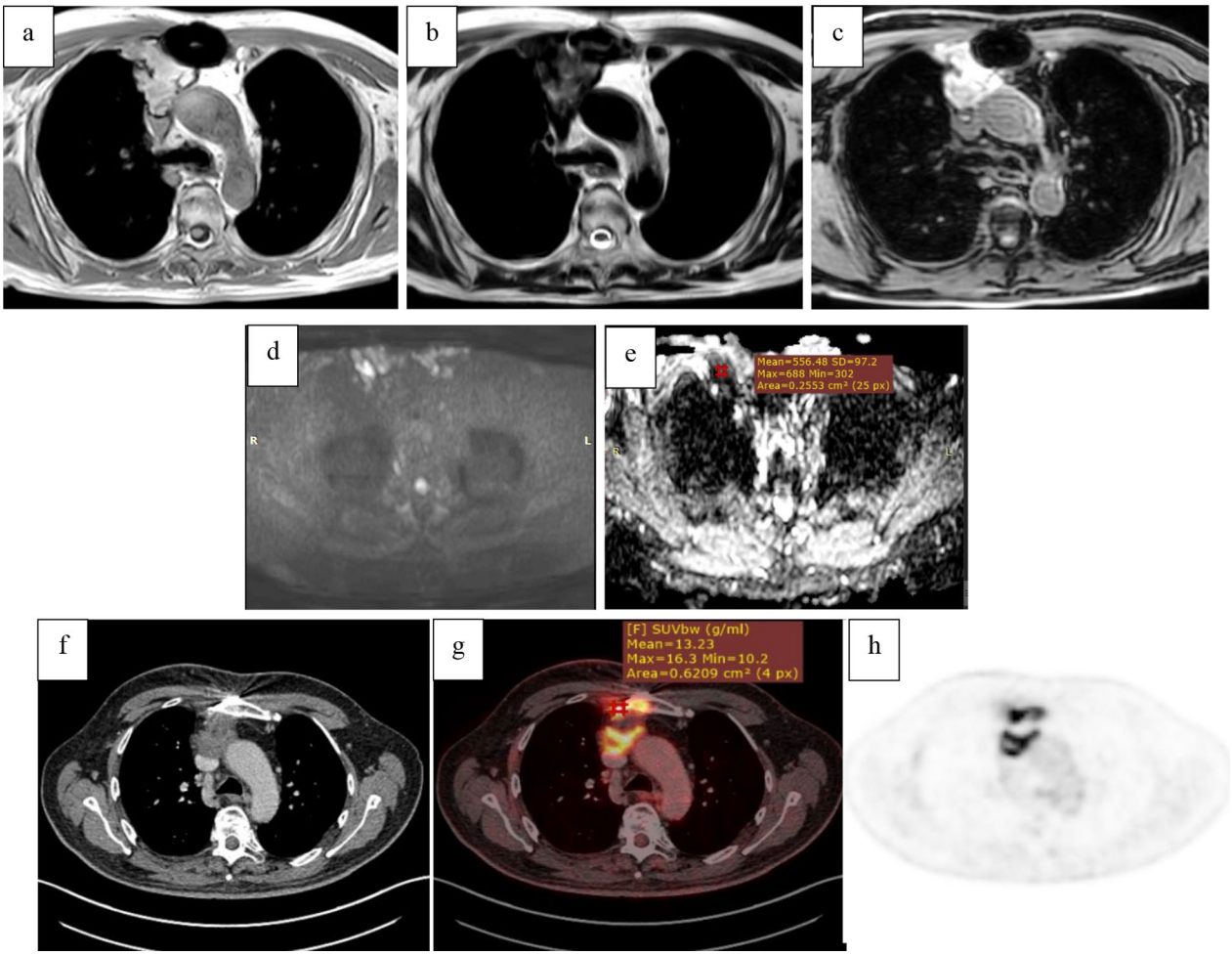

Fig. 8 69-year-old male patient with history of treated differentiated thyroid cancer coming for follow up. MRI chest and PET/CT were performed as part of his investigation profile. **a** Axial T1, **b** axial T2, and **c** post contrast axial T1 fat suppression showing anterior mediastinum/retro-sternal lobulated soft tissue lesion reaching the anterior aspect of the ascending aorta and extending to encircle the right sterno-clavicular joint with periarticular soft tissue sheets. It elicits isointense T1 and heterogeneous iso to low T2 signal intensity with heterogeneous post contrast enhancement. **d** DWI and **e** ADC map showing diffusion restriction in the form of high diffusion signal and low ADC. ADC value = 0.56×10^{-3} mm^2/s. Note metallic susceptibility artifacts from sternotomy wires suture. **f** Axial CT, **g** axial fused PET-CT, and **h** axial PET image showing retrosternal FDG uptake with erosion of the adjacent sternum and right sterno-clavicular joint (SUV = 13.2). CT-guided biopsy revealed nodal metastasis

concluded a sensitivity of 70% and specificity of 87% at cut off value of 3.0 .

Our study showed that ADC and SUV values had an inverse correlation with high SUV and low ADC values observed in malignant tumors (Fig. 8). Our results are compatible with the study conducted by Lee et al. [38], in which 57 patients performed both DW MRI and PET/CT; their results also revealed inverse correlation between the ADC value and SUV measurement, and outlined the usefulness of using ADC and SUV as an adjunct to morphological imaging to enhance the diagnosis, and as a tool for determining response to therapy.

This study has some limitations as it included only a limited number of lesions. Included lesions were histologically variable and each has variable tissue components. Hence, the need for more studies with larger populations, and larger scale randomized controlled trials are needed to validate our results.

Conclusions

In conclusion, both DWI-MRI and PET/CT can reliably differentiate benign from malignant lesions, yet, PET/CT showed higher sensitivity, specificity and accuracy.

So, we recommend DWI-MRI of the chest wall as a non-invasive and radiation-free imaging modality for diagnosis of primary chest wall lesions, to assess their nature and composition, hence, aiding in differentiation between benignity and malignancy. In case of malignancy, this should be followed by PET/CT, which will give an idea about the lesion nature, as well as detect other lesions elsewhere in the body within a single quick whole-body examination for better management decision. However, PET/CT is the optimal imaging modality for staging, restaging, and assessment of therapeutic response.

Abbreviations

ABC	Aneurysmal bone cyst
ADC	Apparent diffusion coefficient
CMF	Chondromyxoid fibroma
DWI	Diffusion weighted images
FDG PET-CT	18F fluorodeoxyglucose positron emission tomography/computed tomography
GCT	Giant cell tumor
LCH	Langerhan cell histocystosis,
MPNST	Malignant peripheral nerve sheath tumor
MRI	Magnetic resonance imaging
OM	Osteomyelitis
PNET	Primitive neuroectodermal tumors
ROI	Region of interest
SUV	Standardized uptake value
TB	Tuberculosis.
UPS	Undifferentiated pleomorphic sarcoma

Acknowledgements
Not applicable.

Author contributions
IHM, AHM and YYS reviewed the images. SFT, AHM, HZ, YYS, YHE, MAK and MRA analyzed and interpreted the patient data. AAH did the statistical analysis, SFT wrote the manuscript and YYS reviewed it. All authors have read and approved the manuscript.

Funding
The authors state that this work has not received any funding.

Availability of data and materials
The datasets used and/or analyzed during the current study are available from the corresponding author on reasonable request.

Declarations

Ethics approval and consent to participate
Approval of the ethical committee of the 'Radiology department, Faculty of Medicine, Cairo University' was granted before conducting this prospective study; Reference number: MD-98-2021. Local institutional review board approval was granted before conducting this cross sectional study, and written informed consent was obtained from all patients.

Consent for publication
All patients included in this research gave written informed consent to publish the data contained within this study. If the patients were less than 16-year-old, deceased, or unconscious when consent for publication was requested, written informed consent for the publication of this data was given by their parents or legal guardians.

Competing interests
The authors declare that they have no competing interests.

Received: 14 October 2023 Accepted: 17 December 2023
Published online: 03 January 2024

References

1. Bajaj T, Aboeed A (2019) Chest wall tumors
2. Carter BW, Gladish GW (2015) MR imaging of chest wall tumors. Magnet Reson Imaging Clin 23(2):197–215
3. Nam SJ, Kim S, Lim BJ, Yoon CS, Kim TH, Suh JS, Ha DH, Kwon JW, Yoon YC, Chung HW, Sung MS (2011) Imaging of primary chest wall tumors with radiologic-pathologic correlation. Radiographics 31(3):749–770
4. O'Sullivan P, O'Dwyer H, Flint J, Munk PL, Muller N (2007) Soft tissue tumours and mass-like lesions of the chest wall: a pictorial review of CT and MR findings. Br J Radiol 80(955):574–580
5. Stowell J, Martínez-Jiménez S (2018) Imaging of nonneoplastic chest wall pathologies. Diagnostic Imaging for Thoracic Surgery: A Manual for Surgeons and Radiologists, 311–341.
6. Tateishi U, Gladish GW, Kusumoto M, Hasegawa T, Yokoyama R, Tsuchiya R, Moriyama N (2003) Chest wall tumors: radiologic findings and pathologic correlation: part 2. Malignant Tumors. Radiograph 23(6):1491–1508
7. Shah AA, D'Amico TA (2010) Primary chest wall tumors. J Am Coll Surg 210(3):360–366
8. Sabri YY, Nossair EZB, Assal HH, Wahba HS (2020) Role of diffusion weighted MR-imaging in the evaluation of malignant mediastinal lesions. Egypt J Radiol Nuclear Med 51(1):1–16
9. Boellaard R, Delgado-Bolton R, Oyen WJ, Giammarile F, Tatsch K, Eschner W, Verzijlbergen FJ, Barrington SF, Pike LC, Weber WA, Stroobants S (2015) FDG PET/CT: EANM procedure guidelines for tumour imaging: version 2.0. Eur J Nucl Med Mol Imaging 42:328–354
10. Thorwarth D, Beyer T, Boellaard R, de Ruysscher D, Grgic A, Lee JA, Pietrzyk U, Sattler B, Schaefer A, van Elmpt W, Vogel W (2012) Integration of FDG-PET/CT into external beam radiation therapy planning. Nuklearmedizin-NuclearMedicine 51(04):140–153
11. Bueno J, Lichtenberger JP III, Rauch G, Carter BW (2018) MR imaging of primary chest wall neoplasms. Top Magn Reson Imaging 27(2):83–93
12. Hagtvedt T, Seierstad T, Lund KV, Løndalen AM, Bogsrud TV, Smith HJ, Geier OM, Holte H, Aaløkken TM (2015) Diffusion-weighted MRI compared to FDG PET/CT for assessment of early treatment response in lymphoma. Acta Radiol 56(2):152–158
13. Feldman F, van Heertum R, Manos C (2003) 18FDG PET scanning of benign and malignant musculoskeletal lesions. Skeletal Radiol 32(4):201–208
14. Lim HK, Jee WH, Jung JY, Paek MY, Kim I, Jung CK, Chung YG (2018) Intravoxel incoherent motion diffusion-weighted MR imaging for differentiation of benign and malignant musculoskeletal tumours at 3 T. Br J Radiol 91(1082):20170636
15. Lee SK, Jee WH, Jung CK, Chung YG (2020) Multiparametric quantitative analysis of tumor perfusion and diffusion with 3T MRI: differentiation between benign and malignant soft tissue tumors. Br J Radiol 93(1115):20191035
16. Hassanien OA, Younes RL, Dawoud RM (2018) Diffusion weighted MRI of soft tissue masses: can measurement of ADC value help in the differentiation between benign and malignant lesions? Egypt J Radiol Nucl Med 49(3):681–688
17. Dietrich O, Raya JG, Sommer J, Deimling M, Reiser MF, Baur-Melnyk A (2005) A comparative evaluation of a RARE-based single-shot pulse sequence for diffusion-weighted MRI of musculoskeletal soft-tissue tumors. Eur Radiol 15:772–783
18. Einarsdóttir H, Karlsson M, Wejde J, Bauer HC (2004) Diffusion-weighted MRI of soft tissue tumours. Eur Radiol 14:959–963
19. Tsubakimoto M, Yamashiro T, Tsuchiya N, Okada M, Maehara H, Kitsukawa K, Murayama S (2018) MRI findings and demographics of elastofibroma dorsi: assessment of diffusion-weighted imaging and contrast enhancement patterns. Acta Radiol 59(6):709–715
20. Zeitoun R, Khafagy SM, Mahmoud IH, El-Wahab NMA (2020) Radiological evaluation of deep soft tissue fibromatosis, the characteristic MR criteria on conventional and corresponding diffusion-weighted images. Egypt J Radiol Nuclear Med 51(1):1–10
21. Oka K, Yakushiji T, Sato H, Fujimoto T, Hirai T, Yamashita Y, Mizuta H (2011) Usefulness of diffusion-weighted imaging for differentiating between

desmoid tumors and malignant soft tissue tumors. J Magn Reson Imaging 33(1):189–193
22. Pekcevik Y, Kahya MO, Kaya A (2015) Characterization of soft tissue tumors by diffusion-weighted imaging. Iran J Radiol 12(3)
23. Kumar Y, Khaleel M, Boothe E, Awdeh H, Wadhwa V, Chhabra A (2017) Role of diffusion weighted imaging in musculoskeletal infections: current perspectives. Eur Radiol 27:414–423
24. Douis H, Davies MA, Sian P (2016) The role of diffusion-weighted MRI (DWI) in the differentiation of benign from malignant skeletal lesions of the pelvis. Eur J Radiol 85(12):2262–2268
25. Aktas E, Arikan M, ARDIC F, Sahin BS, Togral G, Arıbaş BK (2018) The importance of diffusion ADC values in the evaluation of soft tissue sarcomas after treatment. European Congress Radiol-ESSR 2018
26. Saleh MM, Abdelrahman TM, Madney Y, Mohamed G, Shokry AM, Moustafa AF (2020) Multiparametric MRI with diffusion-weighted imaging in predicting response to chemotherapy in cases of osteosarcoma and Ewing's sarcoma. Br J Radiol 93(1115):20200257
27. Yakushiji T, Oka K, Sato H, Yorimitsu S, Fujimoto T, Yamashita Y, Mizuta H (2009) Characterization of chondroblastic osteosarcoma: Gadolinium-enhanced versus diffusion-weighted MR imaging. J Magnet Reson Imaging Off J Int Soc Mag Reson Med 29(4):895–900
28. Ahlawat S, Blakeley JO, Rodriguez FJ, Fayad LM (2019) Imaging biomarkers for malignant peripheral nerve sheath tumors in neurofibromatosis type 1. Neurology 93(11):e1076–e1084
29. Paternain A, García-Velloso MJ, Rosales JJ, Ezponda A, Soriano I, Elorz M, Rodríguez-Otero P, Aquerreta JD (2020) The utility of ADC value in diffusion-weighted whole-body MRI in the follow-up of patients with multiple myeloma. Correlation study with 18F-FDG PET-CT. European J Radiol 133:109403
30. Surov A, Nagata S, Razek AAA, Tirumani SH, Wienke A, Kahn T (2015) Comparison of ADC values in different malignancies of the skeletal musculature: a multicentric analysis. Skeletal Radiol 44:995–1000
31. Ahlawat S, Khandheria P, Subhawong TK, Fayad LM (2015) Differentiation of benign and malignant skeletal lesions with quantitative diffusion weighted MRI at 3 T. Eur J Radiol 84(6):1091–1097
32. Onishi Y, Kitajima K, Senda M, Sakamoto S, Suzuki K, Maeda T, Yoshikawa T, Ohno Y, Sugimura K (2011) FDG-PET/CT imaging of elastofibroma dorsi. Skeletal Radiol 40:849–853
33. Aoki J, Watanabe H, Shinozaki T, Takagishi K, Ishijima H, Oya N, Sato N, Inoue T, Endo K (2001) FDG PET of primary benign and malignant bone tumors: standardized uptake value in 52 lesions. Radiology 219(3):774–777
34. Feldman F, van Heertum R, Manos C (2003) 18 FDG PET scanning of benign and malignant musculoskeletal lesions. Skeletal Radiol 32:201–208
35. Etchebehere EC, Hobbs BP, Milton DR, Malawi O, Patel S, Benjamin RS, Macapinlac HA (2016) Assessing the role of 18 F-FDG PET and 18 F-FDG PET/CT in the diagnosis of soft tissue musculoskeletal malignancies: a systematic review and meta-analysis. Eur J Nucl Med Mol Imaging 43:860–870
36. Shin DS, Shon OJ, Han DS, Choi JH, Chun KA, Cho IH (2008) The clinical efficacy of 18 F-FDG-PET/CT in benign and malignant musculoskeletal tumors. Ann Nucl Med 22:603–609
37. Ioannidis JP, Lau J (2003) 18F-FDG PET for the diagnosis and grading of soft-tissue sarcoma: a meta-analysis. J Nucl Med 44(5):717–724
38. Lee SY, Jee WH, Yoo IR, Jung JY, Im SA, Chung YG, Kang JH (2019) Comparison of 3T diffusion-weighted MRI and 18F-FDG PET/CT in musculoskeletal tumours: quantitative analysis of apparent diffusion coefficients and standardized uptake values. Br J Radiol 92(1102):20181051

Publisher's Note